

Structural, optical, electrical properties of new hybrid organic–inorganic NLO single crystal: bis(1H-benzotriazole) hexaaqua-zinc bis(sulfate) tetrahydrate (BZS)

A. Priyadharshini¹ · S. Kalainathan¹

Received: 17 October 2016 / Accepted: 9 December 2016 / Published online: 24 December 2016
© Springer Science+Business Media New York 2016

Abstract A new hybrid organic–inorganic nonlinear (NLO) single crystal, Bis(1H-benzotriazole) hexaaqua-zinc bis(sulfate) tetrahydrate (BZS), has been successfully synthesized and the single crystals were grown by slow evaporation solution growth technique (SESG) using Millipore water as a solvent. The structure of the BZS crystal was solved and refined by single-crystal X-ray diffraction and demonstrates that the grown crystals belong to a triclinic system with the space group P-1. The asymmetric part of the titled compound contains isolated organic cation (C₆H₆N₃)₂, metallic cation [Zn(H₂O)₆]²⁺, sulfate anion (SO₄)²⁻ and free H₂O molecules. The interplay between the wide number of intermolecular interaction such as O–H...O, N–H...O, C–H...O and π – π stacking interactions were discussed. The optical transmittance spectrum shows that the crystal is excellent transmittance in the entire Vis–NIR region with the cutoff wavelength at 345 nm. The presences of expected functional groups were identified by Fourier transform infrared spectroscopy. The dielectric measurements were carried out at different temperature in the frequency range 100 Hz–5MHz. Furthermore, the studies of its third-order NLO properties using a Z-scan technique demonstrate that the BZS crystal possesses a strong reverse saturable absorption (RSA) and the self-focusing (SF) nature with large second order hyperpolarizability ($\gamma = 6.24 \times 10^{-34}$ esu). All the results indicate that BZS crystal might be the potential candidate for the third-order NLO applications.

1 Introduction

Nonlinear optical (NLO) materials have attracted extreme attention due to their overwhelming success in the field of optical data transmission, information processing [1], electro-optics, photonic [2, 3], 3D optical data storage [4, 5], telecommunication [6–8], laser and optical power limiting [9]. To meet the need of these applications, NLO materials stand the properties of large optical susceptibilities (χ). In recent year, considerable research effort has been devoted to designing and exploring new NLO materials, and numerous organic and inorganic materials with interesting physic-chemical properties have been studied [10–14]. Generally speaking, typical inorganic NLO crystals have excellent thermal and mechanical properties but possess relatively modest optical nonlinearities because of the lack of delocalization of π -electrons [15]. On the other hand, pure organic NLO crystals have high optical susceptibility, and high laser damaged threshold [16–18] compared to inorganic crystals, but their use in device fabrication is restricted by low optical transparency, poor mechanical and thermal stability, and the infeasibility in growing large single crystals [19–22]. Keeping this in the mind, recently researchers are focusing their attention on the organic–inorganic crystals (also called semi-organic), and organometallics crystals are to carries over the advantages of both organic and inorganic characteristic which exhibit the desirable properties chemical flexibility and high optical nonlinearity [23, 24]. Under this circumstance, the complex type of hybrid organic–inorganics (O–I) crystals with NLO effects are developed which are expected to not only retain high nonlinear optical effects but also cut down some shortages of pure organic crystals. As a matter of fact, the hybrid organic–inorganic compounds leads the way for the development of new materials which provide

✉ S. Kalainathan
kalainathan@yahoo.com

¹ Centre for Crystal Growth, School of Advanced Sciences,
VIT University, Vellore 632 014, India

a wide range of potential application from complementary properties to those of classical material [25–29]. However, chemist's skills play a major role in the elaboration and comprehension of such a kind of materials. To this respect, interesting investigation have been devoted to study the synthesis and characterization of new organic–inorganic hybrid compound by the combination of aromatic heterocyclic amine namely 1H-benzotriazole with zinc sulfate heptahydrate. The hybrid organic–inorganic complex product of (1H-benzotriazole) have been attracted to the third-order NLO properties because of the presence of the dislocation π -electron in the organic part and distortion co-ordinated structure from the inorganic part also favours the improvement of the NLO effect. The particular use of the amine, generally protonated amine acting as structuring agent may improve the structure and feature of the new hybrid material. In this supramolecular crystal structure, the amine cations (from organic part) interact with the inorganic part through weak hydrogen bonds, so that this compound belongs to class I of hybrids [30–32].

In this work, we took 1H-benzotriazole as the organic counter cation with isolated metallic cations $[\text{Zn}(\text{H}_2\text{O})_6]^{2+}$, sulfate anions $(\text{SO}_4)^{2-}$ and free H_2O molecule to form the hybrid material of Bis(1H-benzotriazole) hexaaqua-zinc bis(sulfate) tetrahydrate (BZS). The single crystals of BZS were successfully grown from the aqueous solution by slow evaporation method [33, 34].

To the best of our knowledge, studies on the growth and characterization of BZS have not been reported until now. Hence this paper reports the synthesis and solubility of BZS crystal. In addition, the physicochemical properties of the grown crystals were characterized by single-crystal X-ray diffraction, powder XRD, UV–Vis–NIR, FT-IR, dielectric studies, solid state parameters, and chemical etching studies. The third order NLO optical property of BZS has also been investigated using the Z-scan technique using He-Ne Laser.

2 Experimental procedures

2.1 Synthesis

BZS was synthesized by taking stoichiometric ratio (1:1) of zinc sulfate heptahydrate and 1H-benzotriazole in Millipore

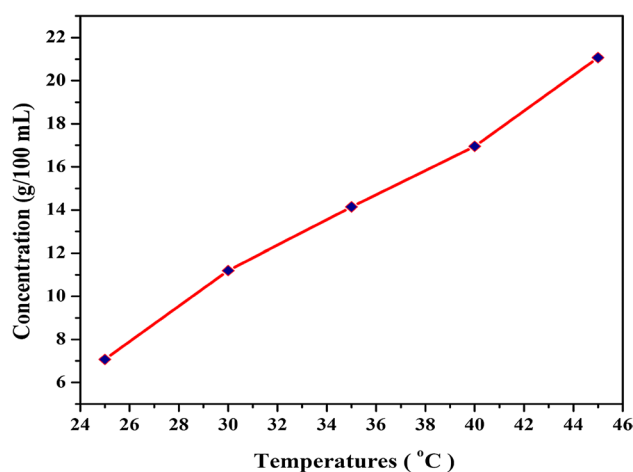
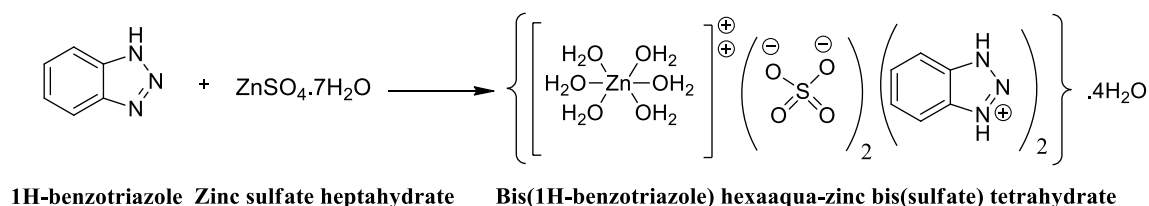


Fig. 1 The temperature dependence of solubility BZS

water (100 mL). The resultant mixture was stirred well at room temperature for 8 h and then filtering, drying at room temperature. The purity of the synthesized material was further improved by repeated recrystallization from Millipore water. The recrystallized material with high purity was used for crystal growth process and further characterization. The reaction scheme of BZS is shown in Scheme 1.

2.2 Solubility

The growth rate of a crystal depends on its solubility and temperature. The solubility of BZS was measured in Millipore water over the temperature range from 25 to 45 °C. Initially, a 150 mL of capacity glass beaker containing 100 mL of Millipore water was placed in the ultra-cryostat temperature bath (accuracy of ± 0.01 °C) and the temperature was set at 25 °C. The powdered sample of BZS was gradually added in Millipore water and stirred by a motorized stirrer. Once attaining the saturation, the equilibrium concentration of the solute was analyzed by gravimetrically [35]. The same procedure was repeated for other temperatures (30, 35, 40, and 45 °C). Figure 1 depicts the solubility of BZS in water as a function of temperature. From the Fig. 1, it is observed that the solubility significantly increases with increasing the temperature, which addressed the high positive solubility and temperature gradient [36, 37].



Scheme 1 Synthesis of BZS

2.3 Crystal growth and morphology

With the help of solubility data, the saturated solution of BZS was prepared in Millipore water at 35 °C (14.142 g/100 mL). The prepared solution was filtered and transferred into 150 mL beaker and tightly covered with aluminium foil with few small holes for slow evaporation and kept in dust free atmosphere. The colorless optically transparent good quality crystals were harvested from the mother solution after a growth period of 42 days. The as-grown crystal is shown in Fig. 2a. The morphology of the BZS crystal was generated from the CIF file (single crystal XRD data as an input) using WinXMOorph software [38, 39]. The predicted morphology of the BZS crystal is shown in Fig. 2b.

3 Results and discussions

3.1 Single crystal X-ray diffraction, data collection and structure determination

A single crystal of BZS with dimensions of $0.32 \times 0.30 \times 0.30$ mm³ was selected and used for the X-ray diffraction analysis. The molecular structure and atomic connectivity of the grown crystal were confirmed through this study. The data set was collected using the Enraf–Nonius CAD-4 diffractometer with graphite monochromated MoK α radiation ($\lambda = 0.71073$ Å) at 293(2) K. The lattice parameters were obtained from a least-square fit. The cell refinement and data reduction were carried out using CAD-4 EXPRESS [40] and XCAD4 [41]. The structure was solved by direct methods as implemented in SHELXS-97 [42] program. The position of all the non-hydrogen atoms was included in the full-matrix least squares refinement using SHELXL-97 [42] package. The crystallographic data and detailed information on the structure refinement for the BZS complex structure were present in Table 1.

The empirical formula for the title compound is $(C_6H_6N_3)_2 [Zn^{II} (H_2O)_6] (SO_4)_2 \cdot 4H_2O$ with the

formula weight 677.93. The cell parameters of BZS crystal are $a = 7.105(5)$ Å, $b = 8.142(6)$ Å, $c = 12.669(3)$ Å, $\alpha = 90.10(1)^\circ$, $\beta = 100.91(2)^\circ$, $\gamma = 111.13(3)^\circ$ and the volume of the unit cell is $669.4(5)$ Å³. It crystallize in the triclinic system with the space group P-1, which is recognized as centrosymmetric that satisfies one of the basics, and essential requirement for the third harmonic generation (THG) activity of the crystal [43–45]. The cif formation of the crystallographic data of the BZS crystal has been deposit with the Cambridge Crystallographic Data Center [CCDC-1453427].

The complex of BZS was synthesized and to form a metal-organic coordination. But surprisingly, the supramolecular BZS crystal structure formed by the alternatively arranged discrete inorganic and the organic layers. The molecular structure of BZS crystal ORTEP [46] views shown in Fig. 3. The inorganic layer containing isolated metallic cations $[Zn(H_2O)_6]^{2+}$, sulfate anions $(SO_4)^{2-}$ and free H₂O molecule and an organic layer formed by the corresponding protonated amines. In the structure, the organic cation is interlayered within the inorganic framework to compensate the negative charge of the inorganic part. In the BZS crystal, Zn²⁺ ion is coordinated with six H₂O molecules forming a slightly distorted octahedral $[Zn(H_2O)_6]^{2+}$ unit. The Zn–O and O–Zn–O bond length and angle are in the range of 2.062(3)–2.112(4) Å and 87.52(16)°–180(1)°, respectively. The sulfate anion adopts the quite regular tetrahedral geometries within which the S–O interaction distance and the O–S–O interaction angle are a ride in the range of 1.465(2)–1.487(3) Å and 108.31(18)–111.6(2). The supramolecular design of the BZS complex is constructed by mean of intermolecular interaction such as O–H...O, N–H...O and weak C–H...O and π – π stacking interactions. Figure 4 shows the ball and stick diagram of BZS. In essence, the structure exhibit the O–H...O hydrogen bond between the inorganic entities, N–H...O hydrogen bond between the inorganic and organic moieties, C–H...O interaction between the organic layer and free water molecule, and the π – π stacking interactions between the aromatic ring of amine groups themselves. Within intermolecular distance, the O–H...O distance varies from 2.706(4) to

Fig. 2 a Harvested crystal of BZS. b Predicted morphology

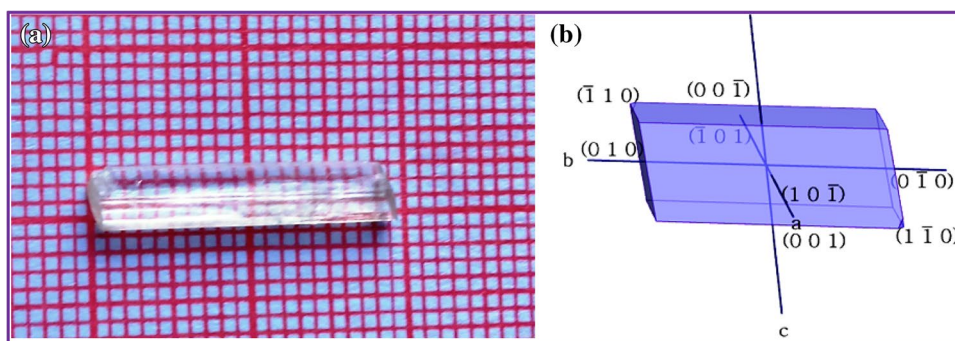
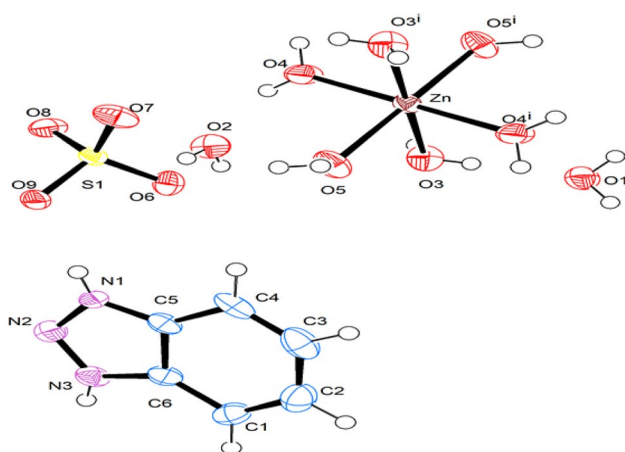
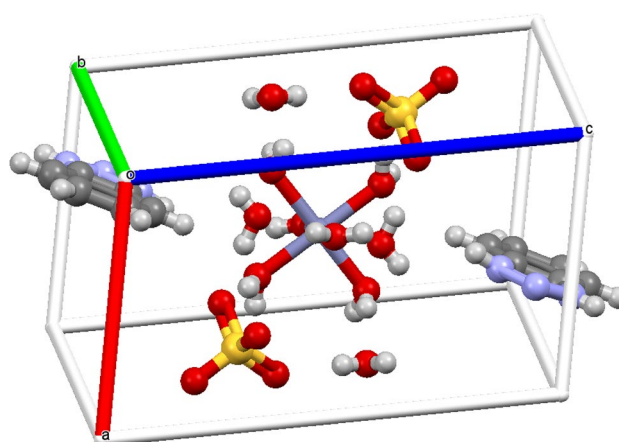


Table 1 Crystal data and structure refinement for BZS complex crystal

Identification code	BZS	
Empirical formula	$C_{12}H_{32}N_6O_{18}S_2Zn$	
Formula weight	677.93	
Temperature	293(2) K	
Wavelength	0.71073 Å	
Crystal system	Triclinic	
Space group	P-1	
Unit cell dimensions	$a = 7.105(5)$ Å	$\alpha = 90.10(1)^\circ$
	$b = 8.142(6)$ Å	$\beta = 100.91(2)^\circ$
	$c = 12.669(3)$ Å	$\gamma = 111.13(3)^\circ$
Volume	$669.4(5)$ Å ³	
Z	1	
Density (calculated)	1.682 Mg/m ³	
Absorption coefficient	1.163 mm ⁻¹	
F(000)	352	
Theta range for data collection	2.69° to 24.96°	
Index ranges	$0 \leq h \leq 8, -1 \leq k \leq 9, -15 \leq l \leq 14$	
Reflections collected	1303	
Independent reflections	1261 [R(int)=0.0355]	
Completeness to theta = 24.96°	99.9%	
Refinement method	Full-matrix least-squares on F ²	
Data/restraints/parameters	1261/0/226	
Goodness-of-fit on F ²	1.161	
Final R indices [I > 2σ(I)]	R1 = 0.0323, wR2 = 0.0867	
R indices (all data)	R1 = 0.0346, wR2 = 0.0891	
Largest diff. peak and hole	0.251 and -0.419 e Å ⁻³	

**Fig. 3** ORTEP drawing for BZS complex crystal

2.823(5) while the N–H...O distance varies from 2.625(5) to 2.661(3). Worthy of mention here is that the π - π aromatic stacking interactions with a face-to-face distance of 3.349 Å between the two stacked rings. The organic cation active its hydrogen atom bonded to the N atoms in N–H...O hydrogen bonds and participates in the structure cohesion through intermolecular H-bonds established between the organic and inorganic layers. The free water molecules

**Fig. 4** Projection of the BZS complex crystal structure

participate in the cohesion of the structure which playing a dual role, one hand they connect sulfates with metallic octahedron and, on the other hand, they connect amines with sulfates. Therefore, they generally ensure a connection between a cationic and an anionic entities. The selected bond length and bond angle are given in Tables 2 and 3 respectively. The list of hydrogen bonds for BZS shown in Table 4.

Powder X-ray diffraction (PXRD) patterns recorded for grown crystal by using BRUKER X-ray diffractometer with CuK α (1.5406 Å) radiation, scanning angle range from 10° to 50° at a scan rate of 0.02 s⁻¹. The obtained diffraction peak (*h k l*) values are indexed by using Powder-X software package. The PXRD patterns are in good agreement with the pattern calculated from a single crystal structure of BZS (Fig. 5), showing that no impurities peaks were observed. It was observed that the appearance of the well-defined sharp and strong peak confirms the good crystallinity of the grown crystal.

3.2 CHN analysis

CHN analysis was performed to determine the percentage of carbon (C), hydrogen (H), and nitrogen (N) in BZS single crystal. The powder sample of the BZS was subjected to this analysis using a Bruker Biospin AG CHN elemental analyzer. The theoretically calculated values are found to be approximately equal to the experimental values (Table 5).

3.3 UV–Vis–NIR spectral analysis

The optical transmission range and lower cut-off wavelength are the vital important optical parameters for NLO applications. The optical transparency (OT) of BZS was recorded in the wavelength range 290–1100 nm with a thickness of 2 mm using ELICO SL 218 double beam UV–Vis–NIR spectrometer. It is noticed that the λ -max value of BZS occur at 345 nm and there is no absorption in the entire Vis–NIR

Table 2 Bond length (Å) for BZS

Atoms	Length	Atoms	Length
Zn–O(4)#1	2.062(3)	N(2)–N(1)	1.319(4)
Zn–O(4)	2.062(3)	O(5)–H(11)	0.84(6)
Zn–O(5)	2.112(3)	O(5)–H(12)	0.86(7)
Zn–O(5)#1	2.112(3)	O(2)–H(10)	0.86(7)
Zn–O(3)	2.112(4)	O(2)–H(9)	0.72(6)
Zn–O(3)#1	2.112(4)	O(3)–H(13)	0.77(9)
S(1)–O(7)	1.465(2)	O(3)–H(14)	0.88(6)
S(1)–O(6)	1.467(5)	N(1)–C(5)	1.332(8)
S(1)–O(8)	1.475(2)	N(1)–H(5)	0.72(5)
S(1)–O(9)	1.484(3)	C(6)–N(3)	1.369(6)
O(4)–H(15)	0.84(5)	C(6)–C(5)	1.395(5)
O(4)–H(16)	0.85(5)	C(6)–C(1)	1.403(9)
C(2)–C(1)	1.357(6)	N(3)–H(6)	0.86(5)
C(2)–C(3)	1.429(7)	C(1)–H(1)	0.9300
C(2)–H(2)	0.9300	C(5)–C(4)	1.408(6)
O(1)–H(7)	0.81(6)	C(4)–C(3)	1.344(10)
O(1)–H(8)	0.84(5)	C(4)–H(4)	0.9300
N(2)–N(3)	1.300(6)	C(3)–H(3)	0.9300

Table 3 Bond angle (°) for BZS

Atoms	Angles	Atoms	Angles
O(4)#1–Zn–O(5)	89.32(14)	O(4)#1–Zn–O(4)	180.000(1)
O(4)#1–Zn–O(5)#1	90.68(14)	O(4)–Zn–O(5)	90.68(14)
O(5)–Zn–O(5)#1	180.000(1)	O(4)–Zn–O(5)#1	89.32(14)
O(4)–Zn–O(3)	90.45(17)	O(4)#1–Zn–O(3)	89.55(17)
O(5)#1–Zn–O(3)	92.48(16)	O(5)–Zn–O(3)	87.52(16)
O(4)–Zn–O(3)#1	89.55(17)	O(4)#1–Zn–O(3)#1	90.45(17)
O(5)#1–Zn–O(3)#1	87.52(16)	O(5)–Zn–O(3)#1	92.48(16)
O(7)–S(1)–O(6)	111.6(2)	O(3)–Zn–O(3)#1	180.000(1)
O(6)–S(1)–O(8)	109.85(19)	O(7)–S(1)–O(8)	109.31(15)
O(6)–S(1)–O(9)	108.31(18)	O(7)–S(1)–O(9)	108.65(16)
Zn–O(4)–H(15)	124(4)	O(8)–S(1)–O(9)	109.12(19)
H(15)–O(4)–H(16)	102(4)	Zn–O(4)–H(16)	130(3)
C(1)–C(2)–H(2)	119.1	C(1)–C(2)–C(3)	121.9(5)
H(7)–O(1)–H(8)	92(5)	C(3)–C(2)–H(2)	119.1
Zn–O(5)–H(11)	125(4)	N(3)–N(2)–N(1)	105.4(4)
H(11)–O(5)–H(12)	90(7)	Zn–O(5)–H(12)	121(3)
Zn–O(3)–H(13)	108(5)	H(10)–O(2)–H(9)	113(5)
H(13)–O(3)–H(14)	100(6)	Zn–O(3)–H(14)	114(4)
N(2)–N(1)–H(5)	119(4)	N(2)–N(1)–C(5)	112.7(4)
N(3)–C(6)–C(5)	104.1(4)	C(5)–N(1)–H(5)	128(4)
C(5)–C(6)–C(1)	122.2(4)	N(3)–C(6)–C(1)	133.7(3)
N(2)–N(3)–H(6)	125(4)	N(2)–N(3)–C(6)	112.3(3)
C(2)–C(1)–C(6)	116.1(4)	C(6)–N(3)–H(6)	121(4)
C(6)–C(1)–H(1)	122.0	C(2)–C(1)–H(1)	122.0
N(1)–C(5)–C(4)	133.8(4)	N(1)–C(5)–C(6)	105.5(4)
C(3)–C(4)–C(5)	116.9(4)	C(6)–C(5)–C(4)	120.7(5)
C(5)–C(4)–H(4)	121.6	C(3)–C(4)–H(4)	121.6
C(4)–C(3)–H(3)	118.9	C(4)–C(3)–C(2)	122.2(4)

region (Fig. 6). The transmittance of 89% is observed from 450 to 1100 nm and it is possibly due to the good crystalline nature of the grown crystal. Hence, this crystal can be a suitable candidate for nonlinear optical application [47].

3.3.1 Determination of optical bandgap (E_g)

The measured transmittance was used to calculate the absorption co-efficient (α) using the following relation

$$\alpha = \frac{2.3026}{t} \log\left(\frac{1}{T}\right), \tag{1}$$

where T is transmittance and t is the thickness of the grown crystal.

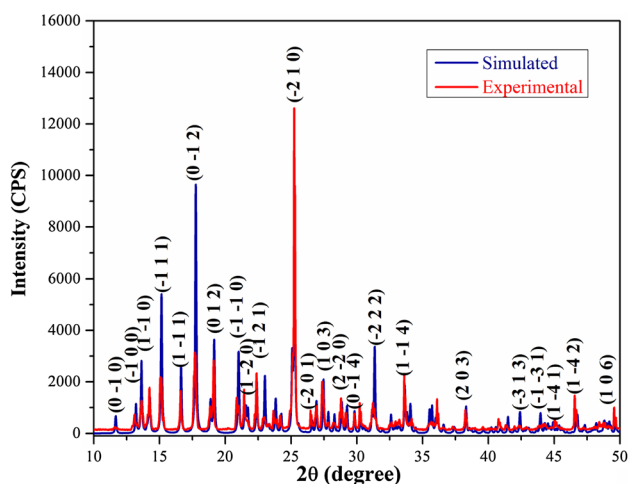
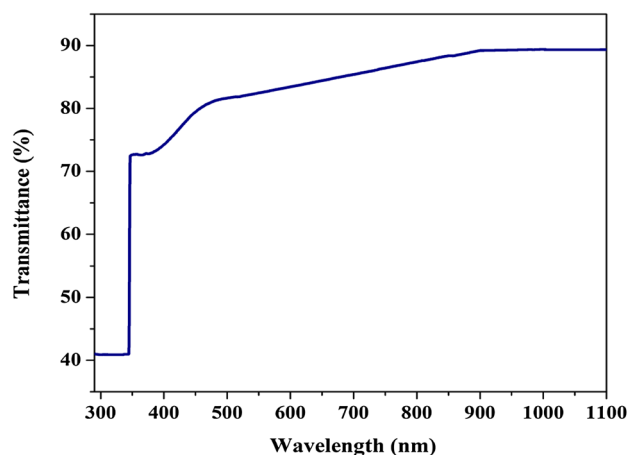
The energy dependence of the absorption coefficient (α) suggests the occurrence of the direct band gap of the BZS crystal obeying the following relation at the high photon energies ($h\nu$) [48, 49],

$$(\alpha h\nu)^2 = A(E_g - h\nu), \tag{2}$$

Table 4 The selected hydrogen bond lengths/Å and angles/° for BZS crystal

Donor-H...Acceptor	d (D-H) (Å)	d (H...A) (Å)	d (D...A) (Å)	<(DHA) (°)
N1-H5...O9 (i)	0.722(4)	1.904(5)	2.625(5)	177.54(5)
N3-H6...O8 (vii)	0.860(4)	1.867(5)	2.661(3)	152.64(4)
O2-H10...O6 (i)	0.857(5)	1.971(6)	2.790(5)	159.73(6)
O5-H12...O6 (i)	0.862(5)	1.899(1)	2.753(5)	170.96(5)
O1-H8...O2 (ii)	0.844(6)	1.898(6)	2.740(5)	176.44(5)
O1-H7...O7 (v)	0.806(6)	1.954(1)	2.736(7)	163.40(6)
O3-H13...O1 (i)	0.768(8)	1.983(9)	2.736(4)	166.79(7)
O5-H11...O1 (iii)	0.839(6)	1.988(6)	2.784(4)	158.14(7)
O4-H15...O8 (vi)	0.842(5)	1.885(5)	2.706(4)	164.81(5)
O2-H9...O9 (iv)	0.721(5)	2.175(7)	2.823(5)	150.28(6)
O4-H16...O2 (i)	0.850(4)	1.990(4)	2.809(14)	161.70(4)
O3-H14...O7 (iv)	0.884(6)	1.991(6)	2.783(5)	168.04(4)

Symmetry codes: (i) x, y, z ; (ii) $x, +y+1, +z$; (iii) $x+1, +y, +z$; (iv) $x-1, +y, +z$; (v) $-x+1, -y+1, z+1$; (vi) $-x+1, -y, -z+1$; (vii) $-x+1, -y, -z$

**Fig. 5** Powder XRD of BZS crystal**Fig. 6** UV-Vis-NIR transmittance spectrum of BZS crystal**Table 5** CHN analysis data

Elements	Theoretical amount (%)	Experimental amount (%)
C	18.16	18.19
H	4.0	4.25
N	10.59	10.68

where A is a constant, h is Planck constant, ν is the frequency of the incident photon, and E_g is the optical band gap. The Tauc's graph [50–52] plotted between $(\alpha h\nu)^2$, and the photon energy ($h\nu$) is shown in Fig. 7. The band gap of the crystal was evaluated by extrapolating the linear part of the graph to the energy axis and is found to be 3.64 eV. However, it is noteworthy that the compound is colourless, the spectrum shows its lower cut-off wavelength in the UV side is about 345 nm, and this indicates that the band gap of the compound is approximately 3.64 eV and the transparent range of BZS is 450 to 1100 nm. Based on these data, the high transmittance (89%) suggest that the BZS crystal offers the low scattering of light (LSL) in the crystal medium from the crystalline defects and the solvent inclusions ensuring the improvement of the optical transparency [53, 54]. As a consequence, the wide range of transparency at the BZS crystal is an added advantage in the field of optoelectronics applications [55, 56].

3.4 FT-IR spectral analysis

The fourier transform infrared spectrum (FT-IR) was recorded using the SHIMADZU instrument by KBr pellet technique in the range from 4000 to 400 cm^{-1} and the recorded spectra is shown in Fig. 8. A broad peak observed at 3284.77 cm^{-1} is due to the O–H symmetric stretching

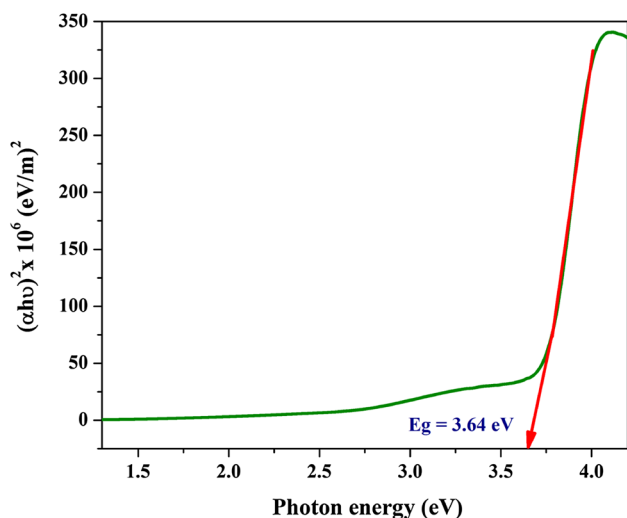
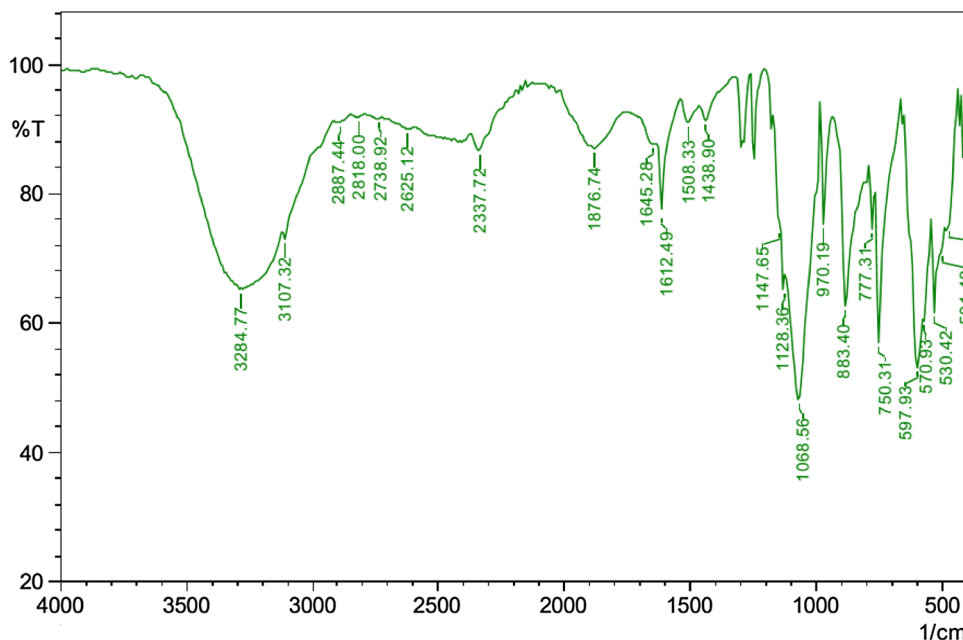


Fig. 7 Plot of $(\alpha h\nu)^2$ against the photon energy (eV)

vibration. The C–H stretching vibration is appeared at 2887.44 cm^{-1} . The band observed at 1645.28 cm^{-1} is due to the N–H bending vibration. The C–O stretching vibration is observed at 1147.65 cm^{-1} . The N–O asymmetric stretching vibrations are observed at 1508.33 cm^{-1} . The C–N stretching vibration was observed at 1128.36 and 1068.56 cm^{-1} . The band at 883.40 cm^{-1} is assigned to be presence of aromatic ring. The peak at 970.19 cm^{-1} is assigned to the C–H bending vibration. The C–H out of plane bending vibration is observed at 777.31 and 750.31 cm^{-1} due to the presence of benzene ring in the benzotriazole. The absorption peak from 501.49 to 597.93 cm^{-1} is due to the characteristic vibration of the SO_4 group stretching. Thus the FT-IR

Fig. 8 FT-IR spectrum of BZS single crystal



transmission spectrum confirms the overall molecular structure of the BZS single crystal.

3.5 Dielectric studies

Dielectric properties are mainly related to the distribution of the electric field within the solid materials. Interestingly, this study provides the quality information of the materials [57]. Dielectric studies of BZS crystal were studied at different temperature (308–338 K) using HIOKI 3532 50 LCR HTESTER meter in the frequency region from 100 Hz to 5 MHz. For this purpose, we selected well transparent crystal with the thickness of 2 mm. The high-grade silver paste was coated on the both the side of the grown crystal and then placed between the two electrodes, and thus uniform ohmic contact was developed on the crystal surface.

The dielectric constant can be calculated using the standard relation,

$$\epsilon' = \frac{Ct}{\epsilon_0 A}, \tag{3}$$

where C and t are the capacitance and the thickness of the crystal, ϵ_0 is the absolute permittivity of free space ($8.854 \times 10^{-12}\text{ F/m}$), A is the area of the cross section of the crystal. The variation of dielectric constant (ϵ_r) and dielectric loss ($\tan \delta$) of BZS crystal as a function of frequency are shown in Figs. 9 and 10 respectively. From the curves, it was observed that the values of the dielectric constant and dielectric loss are gradually decreased with increased frequency. The characteristic of high dielectric constant and dielectric loss at low frequency for a given material suggests that the sample possesses lesser number

of electrically active defects and this parameter is of vital importance for nonlinear optical materials in their application [58]. Hence, the low value of dielectric loss at high frequencies confirms that optical quality of BZS is quite good and thus suitable for photonic, laser, opto-electronic and other nonlinear optical applications [59–63].

3.6 Solid state parameters (SSP) of BZS crystal based on the single crystal XRD data

The value of dielectric constant at high frequency can be used to calculate the Penn gap, Fermi energy and polarisability of the grown crystals [64, 65]. For doing this, additionally, some of the fundamental parameters can be evaluated from the XRD data [66]. The density ρ of the grown crystal is 1.682 Mg/m^3 . The molecular weight M of the BZS crystal is 677.93 g/mol and the total number of the valance of the electron Z is calculated is 232. From the dielectric data the dielectric constant $\epsilon_r = 335$ at 1 MHz for 35°C .

The valence electron plasma energy ($\hbar\omega_p$) is used to determined by using Jackson et al. relation [67],

$$\hbar\omega_p = 28.8 \left(\frac{Z\rho}{M} \right)^{1/2} \quad (4)$$

where $\hbar = h/2\pi$ and ω is plasma angular frequency. The plasma energy in terms of pen gap (E_p) and Fermi energy (E_F) can be obtained from the following relation [68],

$$E_p = \frac{\hbar\omega_p}{(\epsilon_r - 1)^{1/2}}, \quad (5)$$

and

$$E_F = 0.2948(\hbar\omega_p)^{4/3}. \quad (6)$$

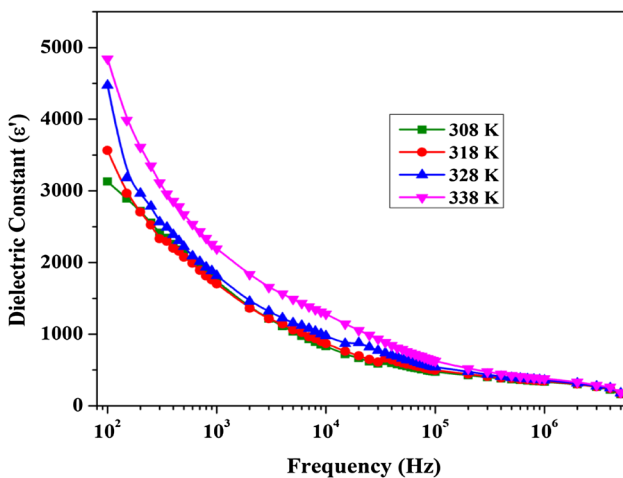


Fig. 9 Variation of dielectric constant with frequency

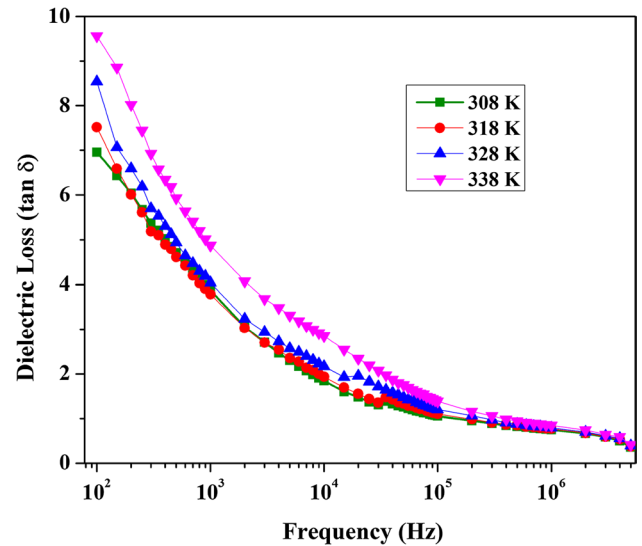


Fig. 10 Variation of dielectric loss ($\tan \delta$) with frequency

Then the electronic polarizability (α) of the grown crystal can be calculated as

$$\alpha = \left[\frac{(\hbar\omega_p)^2 S_0}{(\hbar\omega_p)^2 S_0 + 3E_p^2} \right] \times \frac{M}{\rho} \times 0.396 \times 10^{-24} \text{ cm}^3, \quad (7)$$

where S_0 is the constant for particular materials which can be derived from the below relation

$$S_0 = 1 - \left[\frac{E_p}{4E_F} \right] + \frac{1}{3} \left[\frac{E_p}{4E_F} \right]^2. \quad (8)$$

The obtained value of polarizability (α) from Eq. (7) agrees well with that of the Clausius–Mossotti equation which is given by,

$$\alpha = \frac{3M}{4\pi N_A \rho} \left(\frac{\epsilon_\infty - 1}{\epsilon_\infty - 2} \right), \quad (9)$$

where N_A is the Avogadro’s number ($N_A = 6.023 \times 10^{23}$) and all other symbols are have their own meaning. The value of the electronic polarizability can also be estimated using optical band gap [69]

$$\alpha = \left[1 - \frac{\sqrt{E_g}}{4.06} \right] \times \frac{M}{\rho} \times 0.396 \times 10^{-24} \text{ cm}^3, \quad (10)$$

where E_g is the optical band gap value of the grown crystal. The calculated fundamental data (SSP) of ZSB are compared with the standard KDP crystal [70] as shown in Table 6. From the table, it is observed that SSP of BZS is found to be higher than those of KDP.

3.7 Etching studies

For fabrication of NLO devices, we need good quality crystal with a minimum defect. The chemical etching is an essential study to analyses crystal growth mechanism, structural defect and surface morphology of the grown crystal. Generally, the pattern of the etch pits on the surface of the grown crystal depends on the crystal face, etchant (solvent) used, and an etching time of the crystal. Hence, the presence of etch pits on the surface of the crystal gives the information about the quality of the crystal [71]. A transparent BZS crystal free from the inclusions and cracks was selected for this experiment. Etching analysis was conducted using an optical microscope (Model: Carl Zeiss optical microscope) at a magnification of 50× at room temperature. The etching experiment was carried out on the (0 0 1) plane by using Millipore water as the etchant for 15 and 30 s. The crystal was completely immersed in water for 15 s and then taken out immediately, and then the water on the etched surface was removed gently by using tissue paper, and their microstructures were examined using an optical microscope in reflection mode. Indeed, once the damaged surface layer of the crystal is removed by means of etching, a fresh surface appears which in turn gives clear pits. The photomicrographs of the as-grown and etched surface are shown in Fig. 11a (pre), b (15 s) and c (30 s). It was observed that the size of the etch pits is increased with the increase of etching times while the appeared pit pattern remains same. The average dislocation etch pit density (EPD) was calculated and found to be $1.463 \times 10^3 \text{ cm}^{-2}$ and this was comparable with many crystals [72–74]. The etching study suggests that the grown BZS crystals are of better quality with less dislocation density. The less value of EPD shows that the grown crystal has better crystalline perfection.

3.8 Third-order NLO properties

Single beam Z-scan technique is the most popular method used measured the nonlinear refraction (n_2) and absorption coefficient (β) of the optical materials because of its advantages such as high sensitivity and simplicity. It was

first proposed by Sheik-Bahae et al. [75]. It is a standard method used to evaluate accurately, the real and imaginary part of the third-order nonlinear optical susceptibility (χ^3) and hyperpolarizability (γ) of the BZS single crystal. Here, the most popular He-Ne laser of the wavelength 632.8 nm has been used as the excitations source. The laser of the Gaussian beam profile can be focused by using a convex lens which has the focal length of 30 mm used to produce the diameter of the beam waist ($\omega_0 = 12.05 \text{ }\mu\text{m}$). The essential criteria of the Rayleigh diffraction length (0.72 mm) of the Gaussian beam was calculated using the formula $Z_R = \pi\omega_0^2/\lambda$ (λ is a wavelength in nm). The thickness of the sample is most important to minimize the phase transition in the Z-scan measurement. Here, the sample thickness of 0.68 mm was used for this technique. It should be noted that the thickness of the sample is less than the Rayleigh diffraction length ($L < K = Z_R$, where L is the thickness of the crystal and K is wave vector). When the light was focused on the sample, which is lead to enhance the sample was translated in the +Z to -Z axial direction and the far field intensity was measured as a function of the sample position.

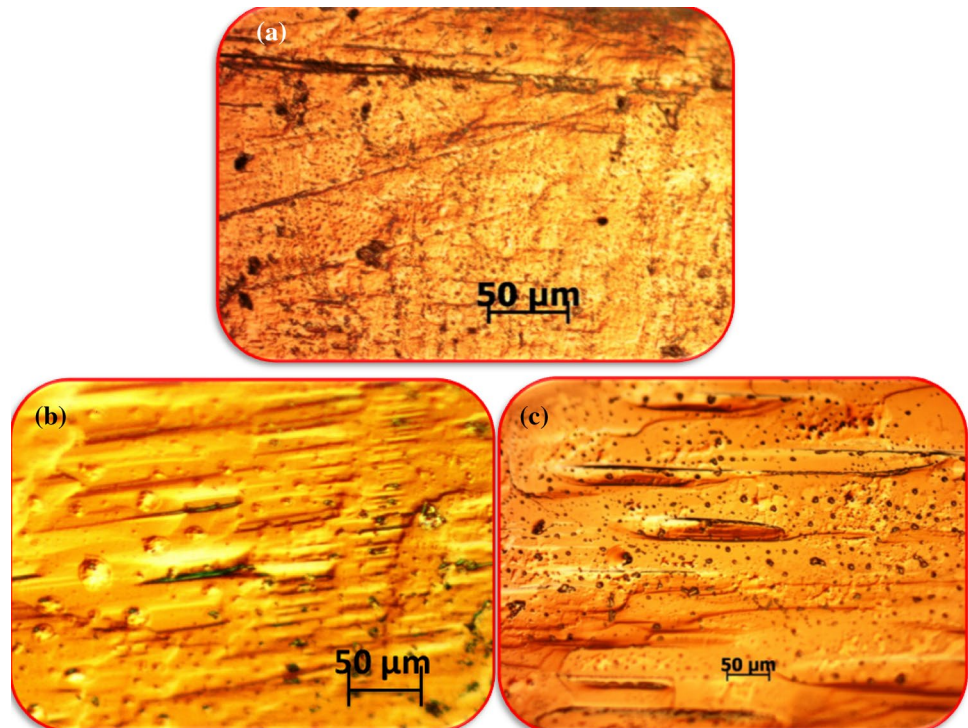
The Z-scan technique is also used to calculate the intensity dependence normalized transmittance. Therefore it is possible to estimate two measurable qualities like nonlinear optical absorption (NLA) and nonlinear optical refraction (NLR). The valuable behaviors of the grown crystal were investigated by the transmission changes with the motion of the sample along the path of a focused laser beam. In the closed aperture elucidate the monitoring transmittance changes through a finite aperture at the far field position, is induced to determine the amplitude of the phase shift ($\Delta\phi$). Whilst in the open aperture, the intensity dependent absorption data were collected by placing the lens in the front of the detector.

The valley to peak pattern of the normalized transmittance observed from BZS crystal using the closed aperture (CA) configuration as shown in Fig. 12. From the CA, it was observed that the valley followed by the peak which corresponds to the positive sign of the nonlinear refraction. This behavior can be attributed the presence of a self-focusing effect in the sample.

Table 6 Some theoretical data for the BZS crystal

Parameters	Values for BZS crystal	Values for KDP crystal
Plasma energy (eV)	21.85	12.27
Penn gap (eV)	1.195	2.07
Fermi energy (eV)	18.00	12.07
Electronic polarizability (α) using Penn analysis	$1.58 \times 10^{-22} \text{ cm}^3$	$4.13 \times 10^{-23} \text{ cm}^3$
Electronic polarizability (α) using Clausius–Mossotti equation	$1.58 \times 10^{-22} \text{ cm}^3$	$4.16 \times 10^{-23} \text{ cm}^3$
Electronic polarizability (α) using optical band gap	$8.46 \times 10^{-23} \text{ cm}^3$	$4.12 \times 10^{-23} \text{ cm}^3$

Fig. 11 Micrograph of the surface of **a** as grown BZS crystal, **b** after 15 s of etching; **c** after 30 s of etching



The difference of the normalized transmittance changes of the valley peak position (ΔT_{p-v}) is evaluated by the following relation,

$$\Delta T_{p-v} = 0.406(1 - S)^{0.25} |\Delta \Phi_o|, \quad (11)$$

where S is denote as linear transmittance aperture and it has been calculated using the standard relation [76],

$$S = 1 - \exp\left(\frac{-2r_a^2}{\omega_a}\right), \quad (12)$$

where r_a is the radius of the aperture and ω_a is the beam radius at the aperture in the linear regime. The nonlinear refractive index (n_2) of the crystal was calculated by using the following relation [77],

$$n_2 = \frac{\Delta \Phi_o}{KI_o L_{eff}}, \quad (13)$$

where $K = 2\pi/\lambda$, ($K = 9.92 \times 10^6 \text{ m}^{-1}$), I_o is the intensity of the laser beam at focus ($I_o = 26.50 \text{ MW/m}^2$) and the effective thickness of the BZS crystal can be estimated as $L_{eff} = [1 - \exp(\alpha L)]/\alpha$, where α is the linear absorption coefficient and L denotes the thickness of the crystal. The open aperture (OA) Z-Scan was employed to calculate the nonlinear optical absorption co-efficient (β) of BZS crystal. The OA curve of BZS (Fig. 13) demonstrates a strong reverse saturable absorption (RSA) indicating a positive

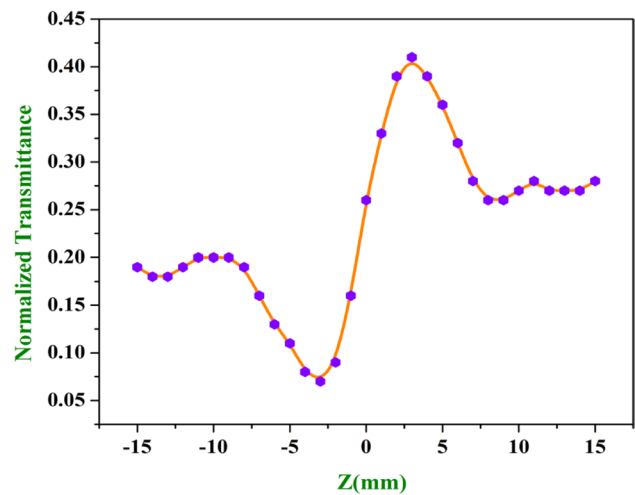


Fig. 12 Z-scan curve of BZS (closed aperture)

absorption coefficient which implying that the crystal effectively used for the optical limiting application such as sensor protection (CCD, human eye etc.) [78]. Hence, the third-order nonlinear absorption co-efficient (β) can be calculated using the following relation [79],

$$\beta = \frac{2\sqrt{2}\Delta T}{I_o L_{eff}}, \quad (14)$$

where ΔT is one valley value present in the open aperture Z-scan curve. The calculated nonlinear refractive index

(n_2) and the nonlinear absorption coefficient (β) of the BZS crystal is $5.2668 \times 10^{-12} \text{ m}^2/\text{W}$ and $1.6423 \times 10^{-4} \text{ m/W}$, respectively. These data are plays a major role to evaluate the real and imaginary part of the third-order nonlinear susceptibility ($\chi^{(3)}$). The real part of the third order nonlinear optical susceptibility $\text{Re}(\chi^{(3)})$ is directly proportional to the n_2 via equation

$$\text{Re}\chi^{(3)}(\text{esu}) = \frac{10^{-4}(\epsilon_0 C^2 n_o^2 n_2)}{\pi} \text{cm}^2 \text{W}^{-1}. \tag{15}$$

And also the imaginary part of the third-order nonlinear optical susceptibility $\text{Im}(\chi^{(3)})$ is related to the β through equation

$$\text{Im}\chi^{(3)}(\text{esu}) = \frac{10^{-2}(\epsilon_0 C^2 n_o \lambda \beta)}{4\pi^2} \text{cm}^2 \text{W}^{-1}, \tag{16}$$

where ϵ_0 is the permittivity of the free space ($8.8518 \times 10^{-12} \text{ F/m}$) and λ is the wavelength of the laser light. In which C and n_o , respectively, are the speed of the light and the linear refractive index of the BZS crystal. Further the Eqs. (15) and (16) express the relation of the third -order nonlinear optical susceptibility (χ^3)

$$|\chi^{(3)}| = \left[(\text{Re}(\chi^{(3)}))^2 + (\text{Im}(\chi^{(3)}))^2 \right]^{1/2}. \tag{17}$$

The second order molecular hyperpolarizability (γ) of the BZS crystal is figured out using the relation [80, 81],

$$\text{Re}[\gamma] = \frac{\text{Re}[\chi^{(3)}]}{Nf^4} \tag{18}$$

Here, N is number of molecule per unit volume (in cm^{-3}) and f represents the Lorentz field correction factor and is given by,

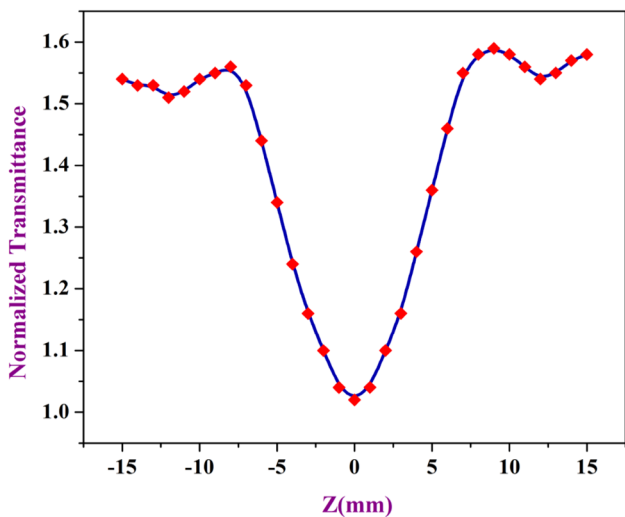


Fig. 13 Z-scan curve of BZS (open aperture)

$$f = \frac{(n_o^2 + 2)}{3}. \tag{19}$$

Generally, two figure of merit $W = n_2 I / \alpha \lambda$ and, $T = \beta \lambda / n_2$ were used to evaluate whether the material can be used as the all-optical switching [82]. Ideally, $W \gg 1$ and $T \ll 1$ for practical device applications. Moreover, in the present case, the calculated value of $W = 2.92$ and $T = 19.73$ for the BZS crystal, does not satisfy the requirement for all-optical switching but may be applied in all optical limiting applications due to its strong reverse absorption saturation (RSA) properties [83]. The measured Z-scan parameters are presented in Table 7. The experimental result shows that BZS crystal possesses great third order nonlinear optical (TONLO) properties. The calculated value of the (β) found to be 1.64×10^{-4} which may due to a large number of delocalized π electron resulting from the present of protonated amine group in the crystal lattice. This delocalization enhances the large value of the third order nonlinear optical susceptibility $\chi^{(3)}$ and second order molecular hyperpolarizability (γ) of the BZS crystal. The large value of third order nonlinear susceptibility $\chi^{(3)}$ BZS crystal is systematically compared with standard KDP and some other NLO compounds tabulated in Table 8. Thus, the obtained results might be a guarantee for the title crystal is a certain candidate for the optical limiting applications.

4 Conclusion

A new hybrid compound of Bis(1H-benzotriazole) hexaaqua-zinc bis(sulfate) tetrahydrate (BZS) has been synthesized for the first time. The single crystals of BZS were successfully grown from the aqueous solution by slow evaporation technique at room temperature. The lattice parameter, crystal system, and the space group were confirmed by single crystal XRD analysis. In this active context, that is to say, a supramolecular structure of BZS is built from unexpected isolated entities $[(C_6H_6N_3)_2 [Zn^{II} (H_2O)_6] (SO_4)_2 \cdot 4H_2O]$. The design of the protonated amine, in the form of 1H-benzotriazole, allowed to forming the weak hydrogen bond from the presence of amine group, and π - π stacking interactions from the aromatic moiety. The UV-Vis-NIR transmittance study reveals that the crystal has good transparency in the entire Vis-NIR region with the lower cut-off wavelength at 345 nm. FT-IR spectral studies confirm the presence of various functional groups in BZS. Low value of dielectric constant (ϵ_r) and dielectric loss ($\tan \delta$) at high-frequency range indicates the suitability of material for the optoelectronic, photonic and NLO devices applications. The electrical polarizability (α) of grown crystal was calculated by Penn analysis ($15.81 \times 10^{-23} \text{ cm}^3$) and Clausius-Mossotti

Table 7 Measurement details and calculated results of the Z-scan technique

Parameters	Measured value for BZS crystal
Laser beam wavelength (λ)	632.8 nm
Lens focal length (f)	30 mm
Aperture radius (r_a)	1.5 mm
Sample thickness (L)	0.68 mm
Effective thickness of the sample (L_{eff})	0.66×10^{-3} m
Nonlinear refractive index (n_2)	$5.27 \times 10^{-12} \text{ m}^2 \text{ W}^{-1}$
Nonlinear absorption coefficient (β)	$1.64 \times 10^{-4} \text{ mW}^{-1}$
Real part of the third-order susceptibility [$\text{Re}(\chi^{(3)})$]	2.60×10^{-6} esu
Imaginary part of the third-order susceptibility [$\text{Im}(\chi^{(3)})$]	3.86×10^{-4} esu
Third-order nonlinear optical susceptibility ($\chi^{(3)}$)	3.86×10^{-4} esu
Second order molecular hyperpolarizability (γ)	6.24×10^{-34} esu
Number of molecules per unit volume	$1.49 \times 10^{27} \text{ m}^{-3}$

Table 8 The value of third order nonlinear susceptibility ($\chi^{(3)}$) compared with standard KDP and some of other NLO compounds

Crystals name	Third order nonlinear optical susceptibility ($\chi^{(3)}$)	References
BZS	3.86×10^{-4} esu	Present work
CBTC	3.56×10^{-5} esu	[84]
ZTS	3.50×10^{-6} esu	[85]
BTZA	1.67×10^{-6} esu	[86]
BTCF	1.38×10^{-8} esu	[87]
KDP	4.02×10^{-14} esu	[88]

Eq. ($15.84 \times 10^{-23} \text{ cm}^3$) found to be having nearly same value. The third-order NLO properties was investigated for the grown crystal by Z-scan measurement and it reveals that the BZS has a strong reverse saturable absorption (RSA) with β of $1.64 \times 10^{-4} \text{ mW}^{-1}$ and a self-focusing with n_2 of $5.27 \times 10^{-12} \text{ m}^2 \text{ W}^{-1}$. The large value of third-order nonlinear susceptibility $\chi^{(3)}$ (3.86×10^{-4} esu) and Second order molecular hyperpolarizability (γ) 6.24×10^{-34} esu reveals that the evidence for using the material in optoelectronic and nonlinear optical device applications and also considered as suitable material for optical limiting applications.

Acknowledgements The authors would like to express the acknowledgement to VIT management for providing financial support and excellent research facilities.

References

- V.G. Dmitriev, G.G. Gurzadyan, D.N. Nikogosyan, *Handbook of nonlinear optical crystals*, (Springer, 2013)
- C. Zhang, Y.L. Song, X. Wang, *Coord. Chem. Rev.* **251**, 111 (2007)
- P.N. Prasad, D.J. Williams, *Introduction to Nonlinear Optical Effect in Molecules and Polymers* (Wiley, New York, 1991), pp. 2–10
- W. Denk, J.H. Strickler, W.W. Webb, *Science* **248**, 73–76 (1990)
- C.C. Corredor, Z.L. Huang, K.D. Belfield, A.R. Morale, M.V. Bondar, *Chem. Mater* **19**, 5165–5173 (2007)
- D.S. Chemla, J. Zyss, *Nonlinear Optical Properties of Organic Molecules and Crystals*, vol. 1. (Academic Press, London, 1987)
- J. Zyss, *Molecular Nonlinear Optics: Materials Physics and Devices*, (Academic Press, New York, Physics and Devices, 1993).
- J. Badan, R. Hierle, A. Perigand, J. Zyss, in *Nonlinear Optical Properties of Organic Molecules and Polymeric Materials*, 233 D.5, ed. by D.J. Williams (American Chemical Society, Washington, DC, 1993)
- C.Q. Tang, Q. Zheng, H.M. Zhu, L.X. Wang, S.C. Chen, E. Ma, X.Y. Chen, *J. Mater. Chem. C* **1**, 1771–1780 (2013)
- X. Liu, X. Wang, X. Yin, S. Liu, W. He, L. Zhu, G. Zhang, D. Xu, *Cryst. Eng. Commun.* **16**, 930–938 (2014)
- W. Zhang, X. Tao, C. Zhang, H. Zhang, M. Jiang, *Cryst. Growth Des.* **9**, 2633–2636 (2009)
- L. Kang, Z. Lin, J. Qin, C. Chen, *Sci. Rep.* **3**, 1366 (2012)
- H.J. Zhao, Y.F. Zhang, L. Chen, *J. Am. Chem. Soc.* **134**, 1993–1995 (2012)
- D. Yuan, Z. Jia, J. Wang, Z. Gao, J. Zhang, X. Fu, J. Shu, Y. Yin, Q. Hu, X. Tao, *Cryst. Eng. Commun.* **16**, 4008–4015 (2014)
- N. Goel, N. Sinha, B. Kumar, *Mater. Res. Bull.* **48**, 1632–1636 (2013)
- W. Zhang, R.-G. Xiong, *Chem. Rev.* **112**, 1163–1195 (2011)
- H. Zhao, Z.-R. Qu, H.-Y. Ye, R.-G. Xiong, *Chem. Soc. Rev.* **37**, 84–100 (2008)
- Z. Sun, S. Li, S. Zhang, F. Deng, M. Hong, *Adv. J. Luo, Opt. Mater.* **2**, 1199–1205 (2014)
- H.O. Marcy, M.J. Rosker, L.F. Warren, P.H. Cunningham, C.A. Thomas, L.A. Deloach, S.P. Velsko, C.A. Ebberts, J.H. Liao, M.G. Kanatzidis, *Opt. Lett.* **20**, 252–254 (1995)
- R. Mohan Kumar, D. Rajan Babu, G. Ravi, R. Jayavel, *J. Cryst. Growth* **250**, 113–117 (2003).
- J. Zyss, D.S. Chemla, *Nonlinear Optical Properties of Organic Molecules and Crystals*. (Academic Press, Orlando, 1986)
- K. Ozga, V. Krishnakumar, I.V. Kityk, J. Jasik-Ślezak, *Mater. Lett.* **62**, 4597–4600 (2008)
- R. Masse, J. Zyss, European Patent EP 0 488 869 B1, (1996)
- C.N.R. Rao, A. Cheetham, A. Thirumurugan, *J. Phys. Condens. Matter.* **20**, 083202 (2008)
- C. Sanchez, B. Julian, P. Belleville, M. Popall, *J. Mater. Chem.* **15**, 3559–3592 (2005)

26. L. Mohana Reddy, S.R. Gowda, M.M. Shaijumon, P.M. Ajayan, *Adv. Mater.* **24**, 5045–5064 (2012)
27. C. Sanchez, P. Belleville, M. Popall, L. Nicole, *Chem. Soc. Rev.* **40**, 696–753 (2011)
28. A. Dolbecq, E. Dumas, C.R. Mayer, P. Mialane, *Chem. Rev.* **110**, 6009–6048 (2010)
29. O. Kammoun, T. Bataille, A. Lucas, V. Dorcet, I. Marlart, W. Rekik, H. Naili, T. Mhiri, *Inorg. Chem.* **53**, 2619–2627 (2014)
30. C. Sanchez, B. Lebeau, *Pure Appl. Opt. J. Eur. Opt. Soc. Part A* **5**(5), 689 (1996)
31. P. Judeinstein, C. Sanchez, *J. Mater. Chem.* **6**(4), 511–525 (1996)
32. P. Gómez-Romero, C. Sanchez eds., *Functional hybrid materials*. (Wiley, 2006)
33. V. Ramesh, K. Rajarajan, *Appl. Phys. B.* **113**(1), 99–106 (2013)
34. R. Surekha, R. Gunaseelan, P. Sagayaraj, K. Ambujam, *Cryst. Eng. Commun.* **16**(34), 7979–7989 (2014)
35. W.S. Wang, K. Sutter, C. Bosshard, Z. Pan, H. Arend, P. Gunter, G. Chapius, F. Nicolo, *Jpn. J. Appl. Phys.* **27**, 1138 (1998)
36. J. Uma, V. Rajendran, *Mater. Int. Prog. Nat. Sci.* **26**, 24–31 (2016)
37. T. Dhanabal, G. Amirthagesan, M. Dhandapani, S.K. Das, *J. Chem. Sci.* **124**, 951–961 (2012)
38. W. J. Kaminsky, *J. Appl. Crystallogr.* **38**, 566 (2005)
39. W.J. Kaminsky, *J. Appl. Crystallogr.* **40**, 382 (2007)
40. Enraf–Nonius, CAD-4 EXPRESS Version 5.1/1.2., Enraf–Nonius, Delft, The Netherlands, 1994
41. A.C.T. North, D.C. Phillips, F.S. Mathews, *Acta Cryst. Sect. A.* **24**, 35 (1968)
42. G.M. Sheldrick, SHELXL97 and SHELXS97, University of Göttingen, Germany, 1997
43. P. Arthi, M. Sumithra Devi, K. Thamizharasan, *J. Solid State Phys.* **2014**, 153272 (2014)
44. E. Corao, S. Baggio, *Inorg. Chim. Acta* **3**, 617–622 (1969)
45. M. Weismann, N.C. Panoiu (2016)
46. L.J. Farrugia, *J. Appl. Cryst. B* **30**, 565 (1997)
47. V. Kannan, R. Bairava Ganesh, P. Ramasamy, *Cryst. Growth Des.* **6**, 1876–1880 (2006)
48. A. Ashour, N. El-Kadry, S.A. Mahmoud, *Thin Solid Films* **269**, 117–120 (1995)
49. G. Saravana Kumar, P. Murugakoothan, *Spectrochim. Acta Part A Mol. Biomol. Spectrosc.* **131**, 17–21 (2014)
50. J. Tauc ed. *Amorphous and liquid semiconductor*, (Plenum Press, New York, 1974), p. 159
51. S. Sirohi, T. P. Sharma, *Opt. Mater.* **13**(2), 267–269 (1999)
52. J. Tauc, R. Grigorovici, A. Vancu, *Phys. Status Solidi B* **15**, 627–637 (1966)
53. N. N. Shejwal, S. Mohd Anis, S. Hussaini, M. D. Shirsat, *Optik* **127**(16), 6525–6531 (2016)
54. D.O. Eya, A.J. Ekpunobi, C.E. Okeke, *Acad. Open Internet J.* **17**, 1–10 (2006)
55. R. Bairava Ganesh, V. Kannan, R. Sathyalakshmi, P. Ramasamy, *Mater. Lett.* **61**, 706 (2007)
56. S. A. Venus, S. Anbarasu, P. A. Devarajan, *Optik* **126**(23), 4561–4565 (2015)
57. C. Balarew, R. Duhlew, *J. Solid State Chem.* **55**, 1–6 (1984)
58. K. V. Rao, A. Smakula, *J. App. Phys.* **36**(6), 2031–2038 (1965)
59. R.S. Narang, B.S. Shah, J.N. Sherwood, *J. Cryst. Growth* **22**, 201–209 (1974)
60. A. Subashini, G. Bhagavannarayana, K. Ramamurthi, *Spectrochim. Acta Part A* **82**, 91–96 (2011)
61. P. Nagapandiselvi, C. Baby, J. R. Gopalakrishnan, *Mol. Struct.* **1056**, 110–120 (2014)
62. K. Sangwal, *Etching of Crystals*, (North Holland Physics Publishing, Amsterdam, 1987)
63. K. Ambujam, P. C. Thomas, S. Aruna, D. P. Anand, P. Sagayaraj, *Mater. Manuf. Process.* **22**(3), 346–350 (2007)
64. K.M. Chauhan, S.K. Arora, *Cryst. Res. Technol.* **44**, 189–196 (2009)
65. P. Balamurugaraj, S. Suresh, P. Koteeswari, J. P. Mani, *Mater. Phys. Chem.* **1**, 4–8 (2013)
66. G. Ganesh, A. Ramadoss, P.S. Kannan, A. SubbiahPandi, *J. Therm. Anal. Calorim.* **112**, 547 (2013)
67. J.D. Jackson, *Classical Electrodynamics*. (Wiley Eastern, 1978) p. 321
68. J.R. Barsoukov, *Macdonald, Impedance Spectroscopy Theory, Experiment, and Applications*, second edn. (Wiley, New Jersey, 2005)
69. R.R. Reddy, Y. Nazeer Ahammed, M. Ravi Kumar, *J. Phys. Chem. Solids* **56**, 825–829 (1995)
70. S. Sagadevan, *Sci. Postprint* **1**(1), e00026 (2014)
71. J.T.J. Prakash, M. Lawrence, J.F. Vimala, M. Iyanar, *J. Phys. Sci.* **14**, 219–226 (2010)
72. M. Shkir, B. Riscob, K.K. Maurya, V. Ganesh, M.A. Wahab, G. Bhagavannarayana, *J. Cryst. Growth* **312**, 3171–3177 (2010)
73. M. Shkir, B. Riscob, M. Hasmuddin, P. Singh, V. Ganesh, M.A. Wahab, E. Dieguez, G. Bhagavannarayana, *Opt. Mater.* **36**(3), 675–681 (2014)
74. Y. Mori, Y.K. Yap, T. Kamimura, M. Yoshimura, T. Sasaki, *Opt. Mater.* **19**, 1–5 (2002)
75. M. Sheik-Bahae, A.A. Said, T.H. Wei, D.J. Hagan, E.W. Van Stryland, *J. Quant. Electron.* **26**, 760–769 (1990)
76. V.P.N. Nampoore, P. Radhakrishnan, *Opt. Commun.* **281**, 2938–2943 (2008)
77. M. Van Stryland, M. Sheik-Bahae, M.G. Kuzyk, C.W. Dirk, *Characterization Techniques and Tabulations for Organic Non-linear Materials*. (Marcel Dekker Inc. 1998), pp. 655–692
78. K.J. Arun, S. Jayalekshmi, *Optoelectron. Lett.* **7**, 136–138 (2011)
79. M. Sheik-Bahae, A.A. Said, E.W. Van Stryland, *Opt. Lett.* **14**, 955 (1989)
80. J. Zhou, E.Y.B. Pun, P.S. Chung, X.H. Zhang, *Opt. Commun.* **191**, 427 (2001)
81. B. Samoc, Z. Samoc, B. Luther-Davies, Z. Bao, L. Yu, U. Hsieh, J. Scherf, *Opt. Soc. Am. B* **15**, 817 (1998)
82. J.L. Bredas, C. Adant, P. Tackx, A. Persoons, *Chem. Rev.* **94**, 243 (1994)
83. S.V. Rao, P.T. Anusha, T.S. Prashant, D. Swain, S.P. Tewari, *Mater. Sci. Appl.* **0.2**, 299 (2011)
84. M. Anis, S.S. Hussaini, A. Hakeem, M.D. Shirsat, G.G. Muley, *Optik* **127**, 2137–2142 (2016)
85. T.C. Sabari Girisun, S. Dhanuskodi, J. Mangalaraj, D. Phillip, *Curr. Appl. Phys.* **11**, 838–843 (2011)
86. G. Pabitha, R. Dhanasekaran, *Opt. Laser Technol.* **50**, 150–154 (2013)
87. N.N. Shejwal, M. Anis, S.S. Hussaini, M.D. Shirsat, *Phys. Scr.* **89**, 125804–125811 (2014)
88. D. Wang, T. Li, S. Wang, J. Wang, Z. Wang, X. Xu, F. Zhang, *RSC Adv.* **6**(18), 14490–14495 (2016)